

doi:10.15199/48.2021.07.08

SRF Control Strategy based on STFIS Controllers For Single-Stage Four-Leg Transformerless Inverter for Grid-Connected PV system

Abstract. In this paper synchronous reference frame (SRF) control strategy based on a self-tunable fuzzy inference system (STFIS) is proposed to control a four-leg transformerless inverter, is presented. The single-stage inverter is controlled to achieve high performance from the PV system without using any maximum power point technique (MPPT), to inject power into the grid, and to improve the power quality, simultaneously. A Fuzzy controller based on an on-line optimization of a zero-order Takagi-Sugeno fuzzy inference system (FIS) by a back propagation-like algorithm is applied to minimize a cost function that is made up of a quadratic error term and a weight decay term that prevents excessive growth of DC-link and PCC. A detailed design of the STFIS controller parameters is given in detail. Furthermore, a comparison between classical PI and STFIS controllers is provided. The performance test of the proposed single-phase configuration and its control strategies are realized under the presence of severe conditions using Matlab/Simulink.

Streszczenie. W artykule przedstawiono strategię sterowania synchroniczną ramką odniesienia (SRF) w oparciu o samostrajalny system wnioskowania rozmytego (STFIS) do sterowania falownikiem beztransformatorowym. Falownik jednostopniowy jest sterowany w celu uzyskania wysokiej wydajności systemu fotowoltaicznego bez stosowania techniki maksymalnego punktu mocy (MPPT), jednoczesnego wprowadzania mocy do sieci i poprawy jakości energii. Sterownik Fuzzy oparty na optymalizacji on-line systemu wnioskowania rozmytego Takagi-Sugeno (FIS) zerowego rzędu za pomocą algorytmu przypominającego propagację wsteczną jest stosowany w celu zminimalizowania funkcji kosztu, która składa się z kwadratowego składnika błędu i wagi zaniku, który zapobiega nadmiernemu wzrostowi łącza DC i PCC. Szczegółowo podano projekt parametrów sterownika STFIS. Ponadto przedstawiono porównanie między klasycznymi sterownikami PI i STFIS. (Strategia sterowania SRF oparta na sterownikach STFIS dla jednostopniowego falownika beztransformatorowego dla systemu fotowoltaicznego podłączonego do sieci)

Keywords: SRF control, Four-Legs transformerless converter, single-stage converter, STFIS controller, power quality improvement.
Słowa kluczowe: falownik, sterownik STFIS, poprawa jakości energii

Introduction

In the last decade, the power energy demand is rapidly increasing, due to the population and economic growth, especially for large countries. To satisfy this demand, many countries in the world adopted a higher penetration of renewable energies, such as wind turbines and solar photovoltaic systems in their utilities. Compared to wind turbines, solar photovoltaic systems (PVs) can easily install on the roofs of houses and factories, which facilities integration of the generated power into the grid and supplied load locally.

According to, [1], there are many configurations to connect solar photovoltaics to the grid. However, one can use either a single-stage inverter or a two-stage inverter to connect the PVs to the grid [2, 3]. According to the comparison study between the existing configurations for PVs connected to the grid realized by [4], a single-stage configuration is a better view of point efficiency, and for the DC voltage stability, a two-stage configuration is more stable, which leads that the power quality improvement can be achieved correctly using this configuration. Compared to the two-stage converter configuration, single-stage converter employ only one converter and less sensors as detailed in [5, 6]. However, an accurate passive element and controller gain design is required to achieve high performance. Also, to get the maximum power point tracking (MPPT) from the PVs, a selected MPPT technique is required [7]. Generally, the maximum PV voltage should be equal to the reference DC link voltage, which is hard to realize due to the sudden solar irradiation change or shading. This objective is solved in [8], using Lyapunov-based control. This approach is effective but more complex. To reduce the control complexity and its implementation in real-time, active and reactive control based on the proportional-integral controller (PI) is proposed in [9]. The obtained results in [9] show a satisfactory performance

under the presence of selected conditions. Unfortunately, this approach is not tested under sudden variation of solar irradiation and shading. Also, the use of simple PI cannot perform well under sudden variations, which causes divergence of the control.

Many control strategies are proposed in the literature to control the interfacing inverter, such as PQ theory-based control, nonlinear control, indirect and direct control, and SRF control, etc. [10]. Most of the proposed control strategies detailed in [10], employed classical PI controllers, which show poor control performances for an integrating process and large time delay process and can easily be saturated during sudden variation. Also, is very sensitive to the noise caused by nonlinear loads [11]. So gain tuning and additional action such as integration of the anti-windup feedback to avoid saturation issue are suggested in [12, 13]. For better performance, authors in [14], proposed proportional resonant controllers with at-windup feedbacks for the inner and outer control loops to the voltage and frequency control for the standalone system. The obtained results show satisfactory performance under load variation and noise conditions. In [15], an adaptive neuro-fuzzy interference system (ANFIS) controller is suggested for two stage-converter configurations. Regarding, the dynamic response, saturation, and noise issue, the controllers suggested in [14-15], perform well, but they are more complex and require more computation time.

This paper introduces the single-stage configuration transformerless inverter for the grid-connected-PV system, and synchronous reference frame (SRF) based control with a self-tunable fuzzy interface system to achieve the following objectives as, 1)Less power losses due to power conversion, 2)Injection of the generated power from PVs without power quality issues, 3)Stability of DC link and AC voltages in the presence of severe conditions, 4)High PV performance without MPPT technique, 5)Optimal STFIS

controller parameters design to achieve high performance during the transition and in presence of charting signal problems.

System understudy

Figure.1 shows the single-stage configuration transformerless inverter for the grid-connected-PV system under study. It consists of photovoltaic panels connected in series with total output voltage closer to the DC-link voltage connected to the grid through a four-leg two-level converter which is controlled to achieve many tasks, such as, 1)

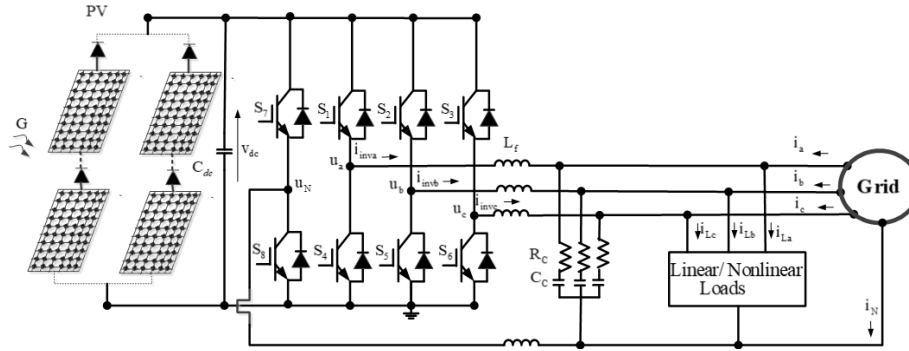


Fig.1. Single-stage four-leg transformerless configuration for grid-connected PV system

Figure.2 demonstrates the characteristics $V_{PV}=f(I_{PV})$ of the selected photovoltaic panels, which are connected in series to get an output voltage closer to the DC link voltage, which is equal to 350 V. As shown in Fig.2 regulating the DC-link voltage at 350 V, one can easily extract the MPPT. This value represents the maximum voltage V_{mp} that extracts if using the conventional MPPT techniques. So, using this concept one can reduce the control system complexity.

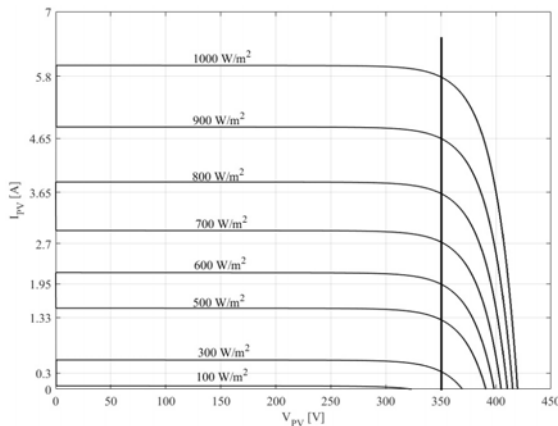


Fig.2. Characteristics $V_{PV}=f(P_{PV})$ and $V_{PV}=f(I_{PV})$ under solar irradiation and fixed temperature

Table 1. PV voltage, solar irradiation, and current

V_{PV} [V]	G [W/m ²]	I_{PV} [A]
350	300	0.3
350	500	1.33
350	600	1.95
350	700	2.7
350	800	3.65
350	900	4.65
350	1000	5.8

Control system

In Figure.3 the enhanced SRF based control based on STFIS controllers proposed in [10] is presented. The load currents (i_{La} , i_{Lb} , i_{Lc}), grid voltages (V_{Ga} , V_{Gb} , V_{Gc}), grid current (i_{Ga} , i_{Gb} , i_{Gc}), DC link voltage (V_{dc}), and neutral current (i_N), of the single-stage converter, are sensed to use as feedbacks signals. With help of the Park's the load currents in the three phases were transformed into dqo frame as,

achieving MPPT by controlling the DC voltage, 2) improving the power quality synchronizing with PCC. RC ripple filter is connected between the four-leg converter and grid to eliminate the ripple voltage due to high-frequency switching. A nonlinear load is connected to the PCC. To allows a three-phase system to use high voltage while still supporting lower voltage single phase application, a neutral wire is used.

$$(1) \begin{bmatrix} i_{Ld} \\ i_{Lq} \\ i_{Lo} \end{bmatrix} = \frac{2}{3} \begin{bmatrix} \cos \theta & -\sin \theta & \frac{1}{2} \\ \cos \left(\theta - \frac{2\pi}{3} \right) & \sin \left(\theta - \frac{2\pi}{3} \right) & \frac{1}{2} \\ \cos \left(\theta + \frac{2\pi}{3} \right) & \sin \left(\theta + \frac{2\pi}{3} \right) & \frac{1}{2} \end{bmatrix} \begin{bmatrix} i_{La} \\ i_{Lb} \\ i_{Lc} \end{bmatrix}$$

where: i_{Ld} , i_{Lq} , and i_{Lo} represent the load currents in the dqo axis.

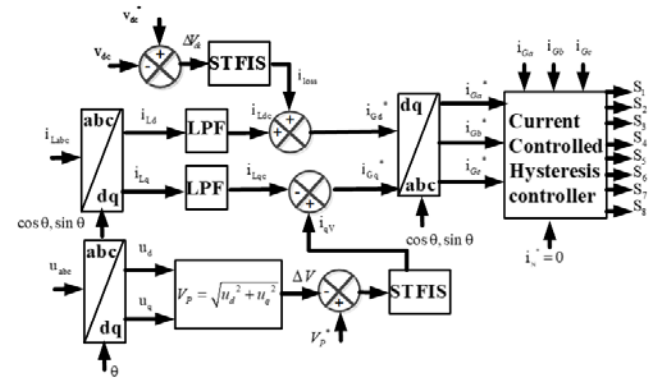


Fig.3. SRF-based control with STFIS controllers

A three-phased locked loop (PLL) is employed to synchronize the signals with grid voltages by calculating $(\cos \theta, \sin \theta)$. The d-q load current components are passed through a low pass filter (LPF) to extract the DC components (i_{Ldc} and i_{Lqc}). The reference of source currents (i_{Gd}^* , i_{Gq}^*) in d-q axis are equal to;

$$(2) \begin{cases} i_{Gd}^* = i_{Ldc} + i_{loss} \\ i_{Gq}^* = i_{Lqc} - i_{lqc} \end{cases}$$

where: i_{Ldc} , i_{Lqc} , i_{loss} , i_{lqc} represent the dq-axis component of the load current; where: i_{loss} , i_{lqc} represent the active and reactive power components, which are obtained at the output of the STFIS controllers of the DC-link and AC voltages.

With help of reverse Park's transformation of the equation in (2), one obtains the references of grid currents (i_{Ga}^* , i_{Gb}^* , i_{Gc}^*) as,

$$(3) \begin{bmatrix} i_{Ga}^* \\ i_{Gb}^* \\ i_{Gc}^* \end{bmatrix} = \frac{2}{3} \begin{bmatrix} \cos\theta & \sin\theta & 1 \\ \cos\left(\theta - \frac{2\pi}{3}\right) & \sin\left(\theta - \frac{2\pi}{3}\right) & 1 \\ \cos\left(\theta + \frac{2\pi}{3}\right) & \sin\left(\theta + \frac{2\pi}{3}\right) & 1 \end{bmatrix} \begin{bmatrix} i_{Gd}^* \\ i_{Gq}^* \\ i_{Go}^* \end{bmatrix}$$

The reference grid currents (i_{Ga}^* , i_{Gb}^* , i_{Gc}^* , i_N^*) and the neutral reference current with respective sensed currents (i_{Ga} , i_{Gb} , i_{Gc} , i_N) are fed to current-controlled hysteresis controllers to generate the switching signals to (S₁-S₈).

STFIS controllers design

As detailed in Fig.2, both outer control loops employed self-tuning fuzzy inference system (STFIS) controllers, which are a neuro-fuzzy network that provides a complete structural system with the fuzzy inference of zero-order type Takagi-Sugeno. Its architecture, which consists of four layers as detailed in [16, 17]. However, the errors in voltage (ΔV and ΔV_{dc}) of the AC and DC voltages are received by the first layer, and the membership degrees of these errors are calculated in layer two. The value of the truth is calculated in the third layer. The fourth layer is designed to provide the outputs, it calculates the values of and the outputs i_{qv} , and i_{loss} . To adjustment of the backpropagation, the gradient method is used. The optimization is conducted entirely online by minimizing a cost function J to generate the parameters w_i , characterizing the conclusion part of rules, and adjust them. However, The gradient descent algorithm with the regression parameters optimizing only the conclusion part of rules is adapted to meet the targets. The cost function is expressed as,

$$(4) \quad J = E + \lambda \sum w^2$$

where: w , λ , and E denote the weight, constant that controls the growth parameters, and the quadratic error, respectively.

With help of the backpropagation method and the effect of the regression term of the weights in the cost function, the parameters are adjusted as,

$$(5) \quad w(t+1) = w(t) + \eta \left(-\frac{\partial J}{\partial w}\right) + b \Delta w(t)$$

With the help of Eq.4 and taking the regression coefficient β equal to $2\lambda\eta$, Eq.5 is rewritten as,

$$(6) \quad w(t+1) = w(t) + \eta \left(-\frac{\partial E}{\partial w}\right) + b \Delta w(t) - \beta w(t)$$

Equation (6) is updated by multiplying the regression coefficient by $\alpha_i / \sum_i \alpha_i$

where α_i is the truth value of the premise part of the triggered rule.

However, one can easily incorporate the effect of the regression terms in the cost function, which is limited for the optimization of the output as,

$$(7) \quad \Delta w_{1j}^4(t) = -\eta \delta_1^4 \alpha_j^3 + b \Delta w_{1j}^4(t-1) - \alpha_j^3 \beta w_{1j}^4(t-1) / \sum \alpha_j^3$$

$$(8) \quad \delta_1^4 = y_1 - y / \sum_j \alpha_j^3$$

Where $w_{ij}^n(t)$: i^{th} is the parameter between i of layer n and j^{st} unit of layer $(n-1)$, α_i , η is the positive learning gain, t is the training iteration, b is the moment

parameter, δ_i^n represents derived term of the cost function (i^{th} neuron of layer n), δ_j^{n-1} is the output of j^{th} unit of layer $(n-1)$, y_1 is the output value, and y represent the dedesired output.

As demonstrated in Fig.4, The Membership functions are normalized and shared in five subsets for all displacement. The linguistic labels are defined as follows: NB: Negative Big, NS: Negative Small, Z approximately Zero, PS: positive Small, and PB: Positive Big. The STFIS network parameters for both outer control loops consist of five memberships functions of type sigmoid and Gaussians, where their parameters are equal to $\beta = 0.0001$, $\eta = 0.3$ and $b = 0.9$.

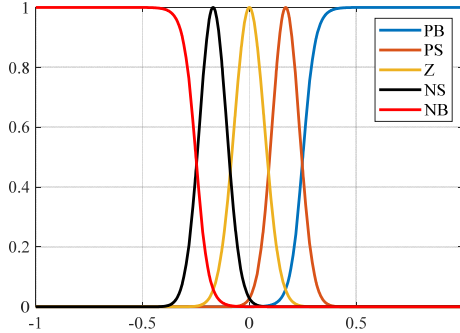


Fig.4. Memberships function

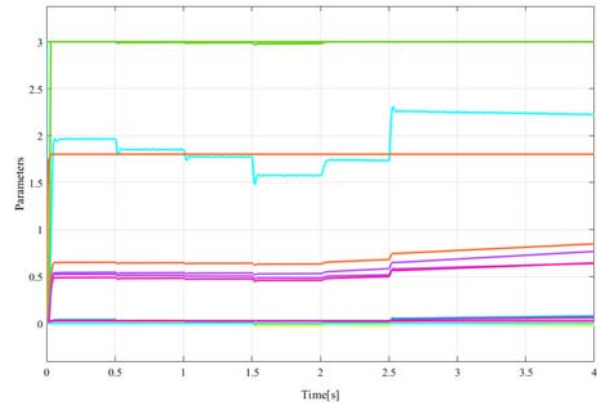


Fig.5. The parameters (weights)

Figure.5 represents the convergence of the parameters (weights) of the four-layer. One observes clearly that the STFIS controllers achieve a good tracking feature during the transition and at steady-state.

Results and discussion

To test the performance of the single-stage transformerless four-leg converter grid-connected PV system and the improved enhanced SRF based-control with STFIS controllers, the system is subjected to sudden solar irradiation and sudden balanced and unbalanced nonlinear load variation.

In Figure.6 the dynamic performance of the grid voltages (V_G), grid currents (i_G), load currents (i_L), inverter currents (i_{inv}), output PVs current (i_{PV}), DC-link voltage (V_{dc}), and its reference (V_{dc}^*), and neutral current (i_N), are demonstrated. System is subjected to sudden solar irradiation at $t=0.4$ s, $t=0.9$ s, $t=1.4$ s, $t=1.9$ s, and at $t=2.4$ s. Also, the system is subjected to the load change at $t=1.9$ s. one observes that DC In link voltage flows it reference during solar irradiation, also the AC voltage is maintained constant during these sudden variations, which confirms the robustness of the STFIS controllers for the outer loops

control. One observes clearly that at $t=1.9$ s the unbalanced nonlinear load is suddenly connected to the PCC that is why the neutral current appears at this time. To balance the grid current due to the unbalance created by the unbalanced nonlinear load, the single-stage four-leg-converter acts as an active filter. The maximum output PVs currents at (0.4s, 0.9s, 1.4s, 1.9s, and 2.4s) are equals to (0.3A, 1.95A, 3.65A, 5.8A, and 1.95A) for solar irradiancies (300 W/m^2 , 600 W/m^2 , 800 W/m^2 , 100 W/m^2 , and 600 W/m^2), which is following the obtained results shown in Fig.2 and detailed in Table.1, which confirms the proposed approach to extract the maximum of currents from PVs with controlling only the DC-link voltage without using any MPPTs technique.

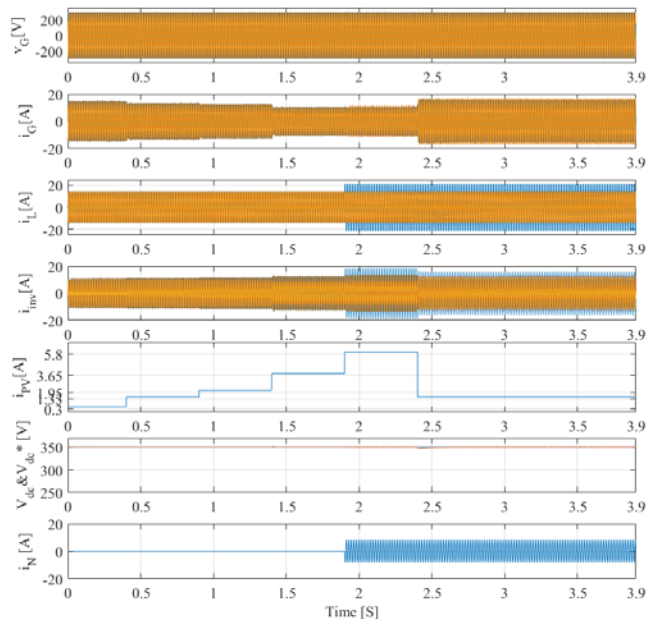


Fig.6. Dynamic performance under load and solar irradiation change

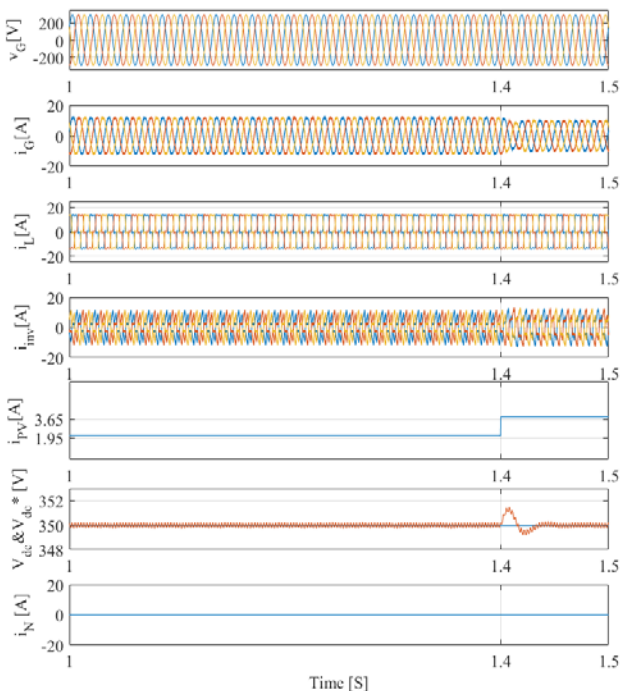


Fig.7. Zoom of the dynamic performance under load and solar irradiation change between $t=1$ s and $t=1.5$ s

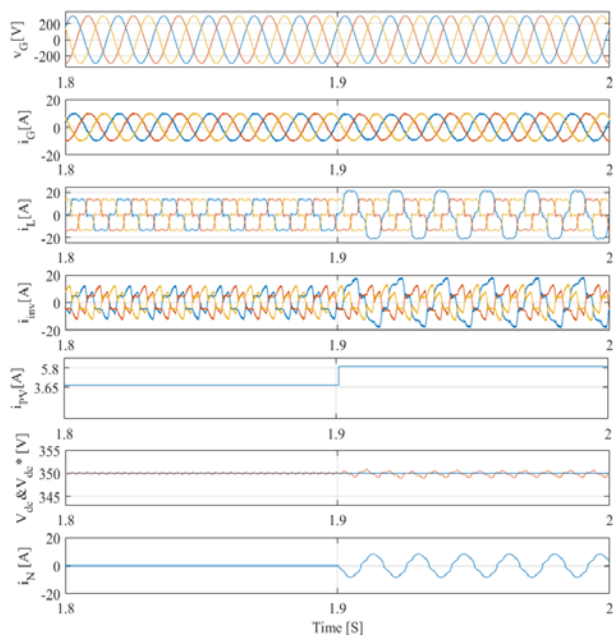


Fig.8. Zoom of the dynamic performance under load and solar irradiation change between $t=1.8$ s and $t=2$ s

In Figure.7 the zoomed waveforms between $t=1$ s to $t=1.5$ s of the performance shown in Fig.4, are presented. One observes clearly that the grid currents are sinusoidal instead of the presence of balanced nonlinear load. One sees that at $t=1.4$ s, the grid currents are decreased due to increasing of the output PV current. The DC link voltage at the sudden variation of solar irradiation from 600 W/m^2 to 800 W/m^2 at $t=1.4$ s is not affected and the overshoot does not exceed 1V, which confirms the robustness of the STFIS regulator to maintain stable the DC link voltage at the sudden variation.

In Figure.8 the zoomed waveforms between $t=1.8$ s and $t=2$ s of the performance shown in Fig.4, are presented. It is observed at $t=1.9$ s the neutral current appears because of the unbalance in load current. Instead of this perturbation, the grid current is balanced and sinusoidal. The DC link voltage and AC voltage are well regulated in this period. Also, the PVs current increases from 3.65 A to 5.8 A due to an increase of the solar irradiation from 800 W/m^2 to 1000 W/m^2 . This confirms the good operation of the enhanced SRF control based STFIS controllers in the presence of unbalanced nonlinear load and sudden variation of solar irradiation.

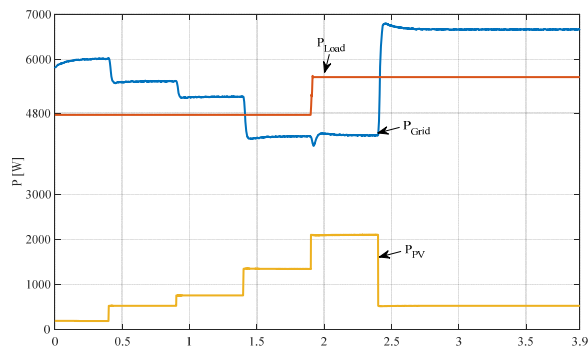


Fig.9. Grid, PVs, and load active powers during variation of load and solar irradiancies

In Figure.9 the waveforms of the active powers of load (P_{Load}), grid (P_{Grid}), and PVs (P_{PV}) are demonstrated. One observes that the grid power varies with the variation of the

output PV currents, It decreases with the increase of the generated power from the PVs. One observes that load is supplied without interruption at all times, which confirms the good operation of the proposed configuration and their control strategies based on STFIS controllers. In Figure.10 the harmonic spectrum of a) load current, b) grid current, and c) the grid voltage, are presented. One observes that the total harmonic distortion of grid current and voltage current is less than 5%, which respects the recommendation harmonics levels in IEEE Std 519-1992.

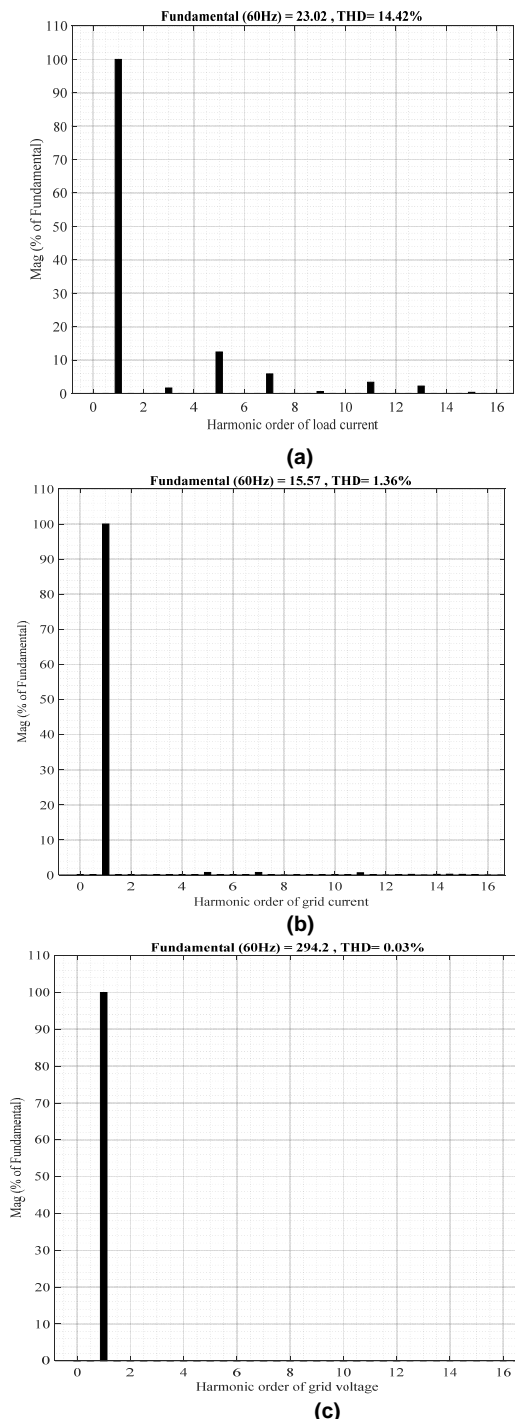


Fig. 10. Harmonic spectrum of a) load current, b) grid current, and c) grid voltage

In Figure.11 (a) the waveforms of the DC link voltage regulation using the STFIS controller and the conventional PI controller is presented. One observes clearly that during the sudden variation of the solar irradiation STFIS controller is more stable than the PI controller, which confirms our

choice for this application that necessitates a stable DC link voltage to extract the MPPT from the PVs. One observes in Fig.11 (b) the THD of the grid current when to use PI controllers are 4.99%, however, in Fig.11 (c) the THD of the grid current when using the STFIS controller is 1.36%. Both THD respects the recommendation of IEEE-519-1992, but that with STFIS controller is perfect.

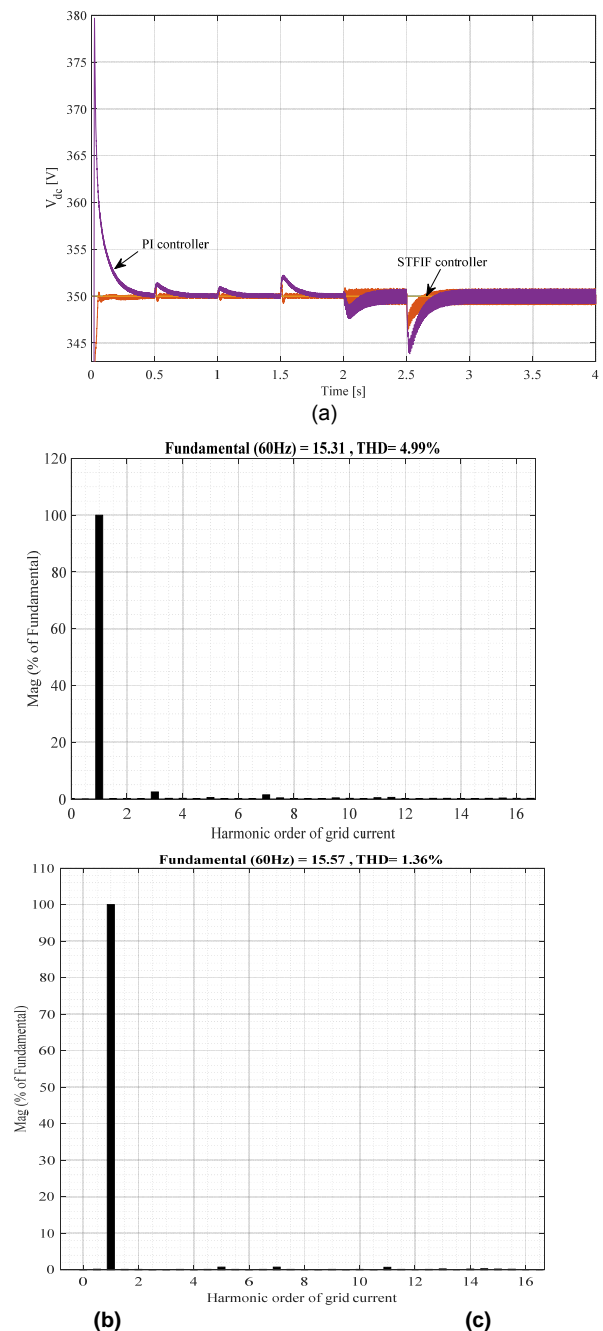


Fig. 11. Harmonic spectrum of a) load current, b) grid current, and c) grid voltage

Conclusion

In this paper single-stage transformerless four-leg converter configuration for grid-connected PVs is selected for low voltage application. Enhanced synchronous reference (SRF) based control with STFIS controllers for DC link voltage and AC voltage regulators, is selected and implemented. An accurate gain design for the STFIS controllers and comparison study SFIS and PI controllers are provided. It has been demonstrating the capability of these advanced controllers to maintain stability under the

presence of noise in the AC and DC voltages. It has been confirmed that one can extract the MPPT from PVs by controlling the DC-link voltage and without using any MPPT methods. The obtained results viewpoint THD and response time under the presence of severe conditions such as solar irradiation and unbalanced nonlinear load are satisfactory.

Authors: dr. Djamel-Eddine Chaouch, Faculty of Science and Technology, University Mustapha Stambouli of Mascara, Algeria E-mail: d.chaouch@univ-mascara.dz; dr. Hocine Abdelhak Azzeddine, LSTE Laboratory, Faculty of Science and Technology, University Mustapha Stambouli of Mascara, Algeria E-mail: hocine.azzeddine@univ-mascara.dz; dr. Ahmed LARBAOUI, Faculty of Science and Technology, University Mustapha Stambouli of Mascara, Algeria E-mail: ahmed.larbaoui@univ-sba.dz; prof. Zoubir Ahmed-Foiti, Faculty of Electrical Engineering, University of Sciences and Technology of Oran, El M^{naouer}, Oran, Algeria, E-mail: zfoitih@yahoo.fr.

REFERENCES

- [1] Ueckerdt, Falko, Robert Brecha, and Gunnar Luderer. "Analyzing major challenges of wind and solar variability in power systems." *Renewable energy* 81 (2015): 1-10
- [2] Islam, Md Rabiul, A. M. Mahfuz-Ur-Rahman, Kashem M. Muttaqi, and Danny Sutanto. "State-of-the-art of the medium-voltage power converter technologies for grid integration of solar photovoltaic power plants." *IEEE Transactions on Energy Conversion* 34, no. 1 (2018): 372-384
- [3] Wu, Tsai-Fu, Chih-Hao Chang, Li-Chiun Lin, and Chia-Ling Kuo. "Power loss comparison of single-and two-stage grid-connected photovoltaic systems." *IEEE Transactions on Energy Conversion* 26, no. 2 (2011): 707-715
- [4] Zhu, Yongli, JianGuo Yao, and Di Wu. "Comparative study of two stages and single stage topologies for grid-tie photovoltaic generation by PSCAD/EMTDC." In 2011 international conference on advanced power system automation and protection, vol. 2, pp. 1304-1309. IEEE, 2011.
- [5] Patel, Hiren, and Vivek Agarwal. "MPPT scheme for a PV-fed single-phase single-stage grid-connected inverter operating in CCM with only one current sensor." *IEEE Transactions on Energy Conversion* 24, no. 1 (2009): 256-263.
- [6] Wu, Tsai-Fu, Chih-Hao Chang, Li-Chiun Lin, and Chia-Ling Kuo. "Power loss comparison of single-and two-stage grid-connected photovoltaic systems." *IEEE Transactions on Energy Conversion* 26, no. 2 (2011): 707-715.
- [7] Jain, Sandeep, and Vivek Agarwal. "Comparison of the performance of maximum power point tracking schemes applied to single-stage grid-connected photovoltaic systems." *IET Electric Power Applications* 1, no. 5 (2007): 753-762.
- [8] Meza, Carlos, Domingo Biel, Dimitri Jeltsema, and Jacquelin MA Scherpen. "Lyapunov-based control scheme for single-phase grid-connected PV central inverters." *IEEE Transactions on control systems technology* 20, no. 2 (2011): 520-529.
- [9] Sreekanth, Thamballa, Narasimhamurthy Lakshminarasamma, and Mahesh K. Mishra. "Grid tied single-stage inverter for low-voltage PV systems with reactive power control." *IET Power Electronics* 11, no. 11 (2018): 1766-1773.
- [10] Singh, Bhim, Ambrish Chandra, and Kamal Al-Haddad. *Power quality: problems and mitigation techniques*. John Wiley & Sons, 2014.
- [11] Yang, Ming, Dian-guo Xu, and Xian-guo Gui. "Review of control system anti-windup design." *Electric Machines and Control* 10, no. 6 (2006): 622.
- [12] Wang, Liuping. "Automatic tuning of PID controllers using frequency sampling filters." *IET Control Theory & Applications* 11, no. 7 (2017): 985-995.
- [13] Rezkallah, Miloud, Abdelhamid Hamadi, Ambrish Chandra, and Bhim Singh. "Design and implementation of active power control with improved P&O method for wind-PV-battery-based standalone generation system." *IEEE Transactions on Industrial Electronics* 65, no. 7 (2017): 5590-5600.
- [14] Rezkallah, Miloud, Ambrish Chandra, Marco Tremblay, and Hussein Ibrahim. "Experimental implementation of an APC with enhanced MPPT for standalone solar photovoltaic based water pumping station." *IEEE Transactions on Sustainable Energy* 10, no. 1 (2018): 181-191.
- [15] Benhalima, S., Chandra, A. and Rezkallah, M., 2019. Real-time experimental implementation of an LMS-adaline-based ANFIS controller to drive PV interfacing power system. *IET Renewable Power Generation*, 13(7), pp.1142-1152.
- [16] H. Maaref, C. Barret, "Progressive Optimization of a Fuzzy Inference System," *IFSA-NAFIPS'2001, Vancouver*, pp.665-679, 2001.
- [17] K. Zemalache, H. Maaref "Intelligent control for a drone by self-tunable fuzzy inference system," *6th international multi-conference on systems, signals and devices, Djerba, Tunisia*, 23-26 March 2009.